



Cite this: *Nanoscale*, 2015, 7, 15814

Shaping and patterning gold nanoparticles *via* micelle templated photochemistry†

F. Kundrat,^a G. Baffou^b and J. Polleux^{*a,c}

Shaping and positioning noble metal nanostructures are essential processes that still require laborious and sophisticated techniques to fabricate functional plasmonic interfaces. The present study reports a simple photochemical approach compatible with micellar nanolithography and photolithography that enables the growth, arrangement and shaping of gold nanoparticles with tuneable plasmonic resonances on glass substrates. Ultraviolet illumination of surfaces coated with gold-loaded micelles leads to the formation of gold nanoparticles with micro/nanometric spatial resolution without requiring any photosensitizers or photoresists. Depending on the extra-micellar chemical environment and the illumination wavelength, block copolymer micelles act as reactive and light-responsive templates, which enable to grow gold deformed nanoparticles (potatoids) and nanorings. Optical characterization reveals that arrays of individual potatoids and rings feature a localized plasmon resonance around 600 and 800 nm, respectively, enhanced photothermal properties and high temperature sustainability, making them ideal platforms for future developments in nanochemistry and biomolecular manipulation controlled by near-infrared-induced heat.

Received 15th July 2015,
Accepted 29th August 2015

DOI: 10.1039/c5nr04751j

www.rsc.org/nanoscale

Introduction

Noble metal nanoparticles significantly moved forward the development of nanosciences over the last two decades due to their remarkable optical properties.¹ In particular, gold nanoparticles feature localized plasmon resonances that enhance light absorption and scattering from visible to infrared frequencies.² Although colloidal gold have been used since ancient times, the establishment of reproducible synthetic methods recently allowed understanding the shape-dependent optical properties of nanoparticles.³ Approaches to obtain extended and uniform distributions of nanoparticles on planar substrates attracted a lot of attention too, as it offers a convenient configuration for fundamental optical studies⁴ and applications in nanocatalysis,⁵ biosensing^{6,7} and phototherapy.^{8,9} It is common to fabricate nanoparticle monolayers using physical means,^{10–12} but most approaches still have significant limitations in simplifying multi-step procedures and

using benchtop facilities. The simple deposition or immobilization of dispersed nano-objects constitutes a scalable and cost-effective way to fabricate plasmonic substrates. However, such approaches do not allow the uniform assembly of particles over macroscopic areas.^{13–20}

Block-copolymer micellar lithography (BCML) has been recognized as a facile method for generating uniform and regular arrays of nanoparticles with sub-30 nm resolution over arbitrarily large areas.^{21,22} Amphiphilic diblock copolymers undergo microphase segregation in solvents selective for one of the two blocks, resulting in the formation of supramolecular structures.²³ It is simple to simultaneously transfer and organize these structures from solution to substrates *via* evaporation-induced self-assembly.²⁴ Upon deposition, the extended and ordered domains of self-assembled block copolymer molecules can be used as a template to selectively control the deposition of inorganic nanoparticles^{18,25,26} and molecular precursors. Many approaches such as thermal evaporation,²⁷ reactive ion etching,²⁸ electrochemical plating,^{29,30} atomic layer deposition,³¹ galvanic displacement,^{32–34} sol-gel chemistry,^{35,36} and plasma reduction^{36–40} have been combined with BCML for the fabrication of quasi-hexagonally organized nanodots and parallel nanowires of various compositions. Especially for gold, these strategies have been successful to design plasmon-based sensors^{18,41} and bioactive substrates.^{42,43} However, tuning the optical properties of substrates made by BCML is difficult as spherical gold

^aMax Planck Institute of Biochemistry, Department of Molecular Medicine, 82152 Martinsried, Germany. E-mail: polleux@biochem.mpg.de

^bFresnel Institute UMR 7249, CNRS, Aix-Marseille Université, Ecole Centrale Marseille, 13013 Marseille, France

^cCenter for NanoScience, Ludwig Maximilian University, 80799 Munich, Germany

†Electronic supplementary information (ESI) available: Additional SEM, TEM and extinction measurements further describe the mechanism of the reported photochemical approach. See DOI: 10.1039/c5nr04751j

nanoparticles only absorb at around 520 nm and micrometre-long nanowires display a broad longitudinal plasmon resonance in the infrared due to their polydispersity in length. In order to tune the optical properties of the substrates within the visible and near-infrared spectral range, adjusting gold nanoparticle morphology is necessary. For this purpose, several groups used immobilized gold nanoparticles acting as seeds to mediate the growth of anisotropic nanostructures.^{44–47} Nevertheless, this strategy only leads to the non-uniform formation of nanoparticles of different morphologies and sizes, as it is not possible to control the crystallographic orientation of the initial metal seeds. Recently, urchin-shaped gold nanoparticles were successfully grown from arrays of spherical nanoparticles.⁴⁸ Although they proved to be reliable substrates for Raman imaging and spectroscopy, the surface plasmon resonance of such nanostructures was neither characterized nor shown to be tuneable.

In this article, we report a straightforward and cost-effective photochemical approach suited to fabricate uniform and robust nanoparticle arrays with adjustable plasmonic resonances on arbitrarily large glass substrates. We first describe the method to photochemically synthesize gold nanoparticles on polymer-coated surfaces. Next, we show that nanoparticle growth can be resolved at the nanoscale by using block copolymer micellar monolayers as reactive and light-responsive templates. In particular, we describe the preparation of quasi-hexagonally organized randomly shaped nanoparticles (hereinafter termed potatooids) and nanorings. Finally, we characterize their optical and photothermal properties in the context of future applications in plasmon-assisted chemistry.

Experimental

Fabrication of gold nanoparticles on homopolymer thin films

Polystyrene (MW 192 000, PS₁₈₄₆, Sigma-Aldrich) and poly(2-vinylpyridine) (MW 159 000, P2VP₁₅₀₇, Sigma-Aldrich) were dissolved at a concentration of 2 mg mL⁻¹ in *o*-xylene and chloroform, respectively. Glass coverslips (Carl Roth) were cleaned in a piranha solution for at least 2 hours, extensively rinsed with MilliQ water and dried under a stream of nitrogen. Homopolymer thin films were prepared by dip-coating a glass coverslip into the previously prepared solutions with a constant velocity equal to 30 mm min⁻¹. A 2.3 μL drop of aqueous solution of gold chloride (1 wt%, 2.5 mM HAuCl₄, Sigma-Aldrich) was placed onto a UV-transparent quartz coverslip (Jena Compu-graphics). The drop was cautiously flattened with the homopolymer coated glass coverslip while preventing the formation of air bubbles, resulting in a spacing of about 10 μm between both interfaces. The sandwiched system was then exposed to deep UV light using a low-pressure dual emission mercury lamp (Heraeus Noblelight GmbH, NIQ 60/35 XL long-life lamp, 254 and 185 nm with an output of 20 and 5 W, respectively). To remove the coverslip from the quartz, the system was placed in a plastic dish filled with water. Once lifted by water, the coverslip is rinsed with water and dried with nitrogen.

Fabrication of gold nanoparticle arrays with various particle morphologies

Polystyrene(102 000)-*block*-poly(2-vinylpyridine)(97 000) (PS₉₈₀-*b*-P2VP₉₂₃) from Polymer Source Inc. was dissolved at room temperature in anhydrous *o*-xylene (Sigma-Aldrich) at a concentration of 1.7 mg mL⁻¹ in a sealed glass vessel. The solution was then stirred for 2 days. Hydrogen tetrachloroaurate(III) trihydrate (HAuCl₄·3H₂O, Sigma-Aldrich) was added to the polymer solution, stirred for 2 days and filtered. The quantity of gold precursor was calculated relative to the number of P2VP units with a loading parameter (*L*) equal to 0.75, *i.e.* 3 molecules of HAuCl₄ for 4 vinylpyridine monomers. Gold-loaded micellar monolayers were prepared by dip-coating a glass coverslip into the previously prepared solutions with a constant velocity equal to 24 mm min⁻¹. A 2.3 μL drop of water or gold aqueous solution was placed onto a UV-transparent quartz coverslip or a photomask (Jena Compu-graphics). The drop was cautiously flattened with the coated glass coverslip. The sandwiched system was then exposed to deep UV light using either a low-pressure dual emission mercury lamp or a monochromatic lamp (NNI 65/35 XL, 254 nm – 20 W) at 5 cm distance for 4 min. To remove the coverslip from the quartz, the system was placed in a plastic dish filled with water. Once lifted by water, the coverslip is rinsed with water and transferred in a 10 mL aqueous solution containing ethanolamine (2 mM, Sigma-Aldrich) and KAuCl₄ (0.1 wt%, *i.e.* 0.25 mM, Sigma-Aldrich) in order to enlarge the photo-deposited gold nanoparticles. To remove the organic compounds, the processed glass coverslip was exposed to oxygen plasma (1 mbar, Power 65%, 1 h, Modele Femto, Diener). Scanning electron measurements were performed with a Dual Beam™ (FIB/SEM) instrument (Quanta 3D FEG, FEI, Hillsboro). The absorbance spectra were acquired in air with a UV Spectrometer PerkinElmer Lambda 19.

Thermal measurements using TIQSI

Temperature measurements were performed by wavefront sensing using quadriwave shearing interferometry (QSI). Using this technique, a plane optical wavefront crosses the region of interest and undergoes a distortion due to the thermal-induced variation of the refractive index of the medium (water in this article). This wavefront distortion is imaged quantitatively using a QSI wavefront analyser. The source was a collimated light emitted diode from *Thorlabs* (reference no M625L2-C1) whose emitting spectrum spans from 600 to 650 nm. The QSI wavefront analyser was purchased from the *Phasics SA* company (reference name: Sid4Bio). Each image presented in this work is the result of the average of 30 wavefront images, corresponding to a whole acquisition time of around 3 seconds.

Results and discussion

A simple photochemical approach to grow gold nanoparticle monolayers

Among the large variety of synthetic methods that allow the preparation of inorganic nanoparticles, photochemical

approaches have been widely used to establish non-toxic and waste free chemical reactions with high spatial resolution in various environments such as glasses, polymer films, micelles, emulsions, biomolecules and living cells.^{49–51} Such synthetic pathways often involve the use of photosensitizing molecules that generate radicals necessary for the effective reduction of metallic precursors. Radical formation can either take place directly upon photo-induced bond cleavage of the photosensitizer or indirectly upon photo-excitation of the sensitizers able to abstract the hydrogen atoms of donor molecules (H-donors), which turn into reducing species.⁴⁹ To simplify the generation of reducing radicals, Scaiano and coworkers recently showed that tetrachloroaurate anions $[\text{AuCl}_4]^-$ act as a sensitizer too, as its photolysis generates chlorine atoms whose reactivity towards hydrogen abstraction is surprisingly effective for synthesizing gold nanoparticles.⁵²

Based on this finding, we immobilized H-donors on glass in order to grow gold nanoparticle monolayers. For this purpose, we tested the reactivity of two different homopolymers such as polystyrene (PS) and poly(2-vinylpyridine) (P2VP). Glass coverslips were coated with a thin polymer layer and a drop of a gold aqueous solution was flattened with a quartz coverslip (Fig. S1a†). Upon 4 min illumination with a low pressure UV lamp (dual emission at 254 nm – 20 W and 185 nm – 5 W), the substrates were characterized by scanning electron microscopy (SEM), which revealed the presence of randomly distributed gold nanoparticles of a few nanometres in diameter (Fig. S1b and c†). Although this procedure is rather effective without requiring any additional photosensitizers, it

does not allow controlling neither nanoparticle organization nor morphology, necessary to tailor the optical properties of plasmonic substrates.

Micelle templated photochemistry to fabricate uniform arrays of gold potatoids

In order to simultaneously synthesize and organize gold nanoparticles on glass coverslips, we chose to work with amphiphilic polystyrene-*block*-poly(2-vinylpyridine) (PS-*b*-P2VP) as H-donor. In apolar solvents, PS-*b*-P2VP molecules form spherical micelles made of a PS shell and a P2VP core.²³ Micelles can play the role of nanocarriers by adding an acidic gold salt, which loads the micellar core with $[\text{AuCl}_4]^-$ by electrostatically interacting with protonated P2VP. Dip-coating a planar substrate into a micellar solution results in the uniform deposition and the assembly of gold-loaded micelles,³⁷ which will be used as reactive templates to fabricate plasmonic nanoparticles. Fig. 1 illustrates the evolution of the nanostructured substrate after each processing step by displaying schematics of the experimental setup and SEM images at different magnifications. Each series of images was taken with the InLens detector of the SEM for imaging the topography of micelles (Fig. S2a†) and the detector for secondary electrons (SE2) to picture the distribution of $[\text{AuCl}_4]^-$ or gold nanoparticles (Fig. 1a and c).⁵³ As gold anions are already present within the micelles, a water drop was flattened with a quartz coverslip on the ordered micellar monolayer to create a 10 μm thick layer between both interfaces. During this step, micelles undergo slight morphological changes and become sporadically sur-

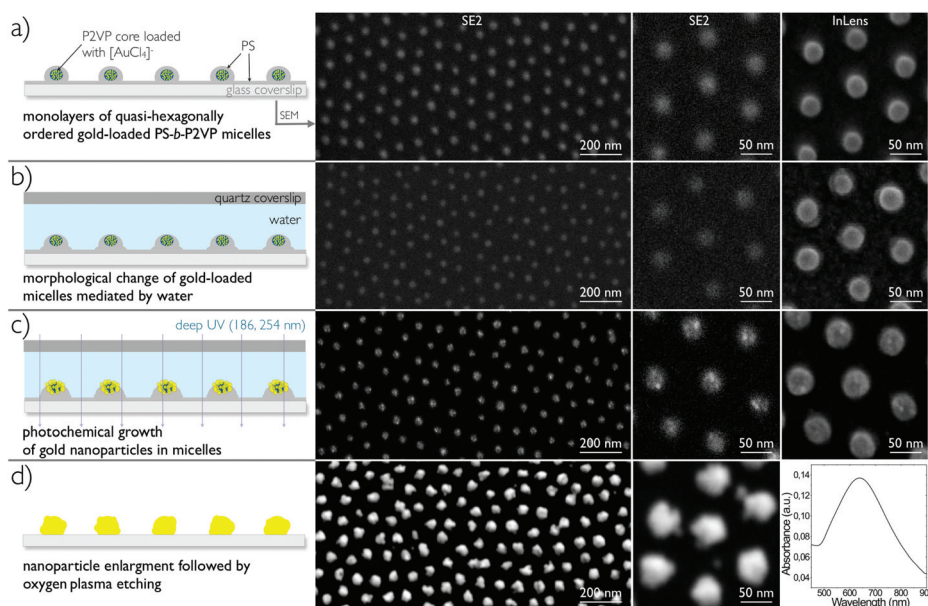


Fig. 1 Micellar photochemical lithography to fabricate randomly shaped gold potatoid arrays. Schematics and SEM images illustrating the evolution of the nanostructured substrate after each processing step: (a) upon dip coating, (b) flattening a water drop, (c) deep UV illumination and (d) electroless deposition followed by O_2 plasma etching. Each series of images was taken with the detector for secondary electrons (SE2) of the SEM to picture the distribution of $[\text{AuCl}_4]^-$ or gold nanoparticles, and with the InLens detector for imaging the topography of micelles, except for (d) where the extinction spectrum measured in air of the gold potatoid array is shown.

rounded by a polymer rim (Fig. 1b InLens). As the morphology of the gold-loaded P2VP cores does not change upon water exposure (Fig. 1b SE2), we suppose that a small structural rearrangement of the PS shell occurred due to its hydrophobic character. It was described that, without the presence of $[\text{AuCl}_4]^-$, PS-*b*-P2VP micellar films become porous upon exposure to polar solvents (Fig. S2b†). During this process, P2VP cores swell, break the upper side of the glassy PS shell and overflow outside the micelles to finally collapse upon drying the substrates.⁵⁴ In our case, micelle opening does not occur as $[\text{AuCl}_4]^-$ stabilizes the protonated P2VP cores. Next, we irradiated the immersed substrate with the UV lamp, which led to the formation of particles of a few nanometres exclusively localized at the micelle position (Fig. 1c). An irradiation time of 4 min was found to be sufficient to generate within individual micelles a few gold particles of about 8 nm in diameter and many gold seeds smaller than 3 nm (Fig. S3†). The preformed particles were then enlarged by electroless deposition (ED) by simply incubating the substrate in a gold aqueous solution in presence of a reducing agent. During ED, the nanoparticles originating from a same micelle increase in size and coalesce into a single particle (Fig. 2). Finally, the substrate was plasma cleaned to etch organic compounds away. With this protocol, we obtained quasi-hexagonally ordered arrays of deformed nanoparticles that we named “potatoids” (Fig. 1d). These arrays feature a nanoparticle interdistance of about 105 nm. With longer ED, the surface plasmon resonance of potatoids becomes more intense and red-shifted due to

their larger size and non-spherical shape. Upon 10, 40 and 90 min of ED, potatoids have an average diameter of 38 ± 7 , 51 ± 11 and 64 ± 12 nm with a plasmon band centred at 582, 614 and 623 nm, respectively, (Fig. 2 and S4a†).

Photochemical nucleation of gold seeds in each micelle followed by particle enlargement constitutes a straightforward two-step approach for reproducibly introducing symmetry breaking in individual nanoparticles and tuning their surface plasmon resonance. For this purpose, it is important to enlarge gold seeds prior to plasma etching because inverting the step order leads to the formation of nanoparticle oligomers with a main absorbance at 540 nm (Fig. S4b and c†). Gold particles smaller than 3 nm are known to be thermodynamically less stable than larger ones,⁵⁵ thereby favouring particle melting and fusion during plasma treatment and then decreasing the number of gold seeds to be grown by ED.

Micropatterning gold potatoids

Photolithography is technologically essential in many applications. As it still requires sophisticated protocols based on the use of photosensitive coating called photoresists, high-throughput preparation of nanoparticle-coated substrates remains limited. In this context, we tested if micelle templated photochemistry was compatible with photoresist-free lithography. To this end, the quartz coverslip was replaced with a quartz photomask coated with a patterned chromium layer used to spatially block UV light and locally control gold growth. In doing so, uniform micropatterned structures of various geometries were successfully fabricated (Fig. 3). The quasi-hexagonal distribution and the irregular morphology of the gold nanoparticles were conserved (Fig. 3d). The smallest pattern size we obtained was about 500 nm (Fig. 3f), which makes this simple procedure more precise than most photoresist- and stamping-based approaches used to spatially control the micrometric distribution of nanoparticles over several centimeters.^{42,56}

Gold nanorings and micelle opening

In an effort to further manipulate the shape of immobilized nanoparticles, we used a gold aqueous solution instead of water to improve the photochemical growth efficiency (Fig. 4a). Surprisingly, instead of generating more nanoparticles per micelle upon UV irradiation, we observed that gold growth occurred at the micelle periphery (Fig. 4b SE2) due to a structure reconstruction from spherical to pitted micelles (Fig. 4b InLens). During ED, gold seeds increase in size and fuse with each other to finally form ring-like structures. Upon plasma treatment, we obtained individual nanorings with an average outer diameter of 56 ± 4 nm and a wall thickness ranging from 9 to 15 nm (Fig. 4c). With this approach each nanoring displays a unique morphology with a structure that is not always fully looped while displaying wall thickness variations originating from the presence of larger seeds. Nevertheless, nanoring morphology and distribution are rather uniform (Fig. S6†) as such substrates feature a near-infrared absorbance centred at around 800 nm (Fig. 4c).

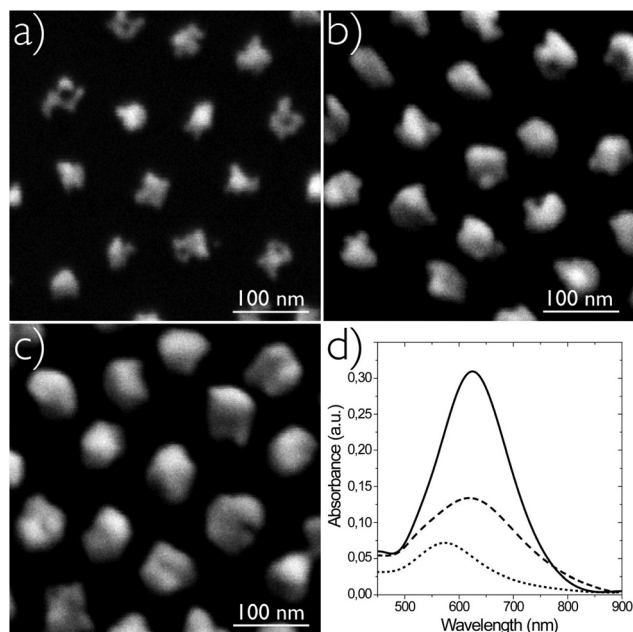


Fig. 2 Tuning the surface plasmon resonance of potatoid arrays with ED time. SEM images of potatoids grown for (a) 10, (b) 40 and (c) 90 min in a mixture of gold aqueous solution and ethanolamine. (d) Extinction spectra measured in air of gold potatoids grown for 10 (dots), 40 (dashes) and 90 min (line).

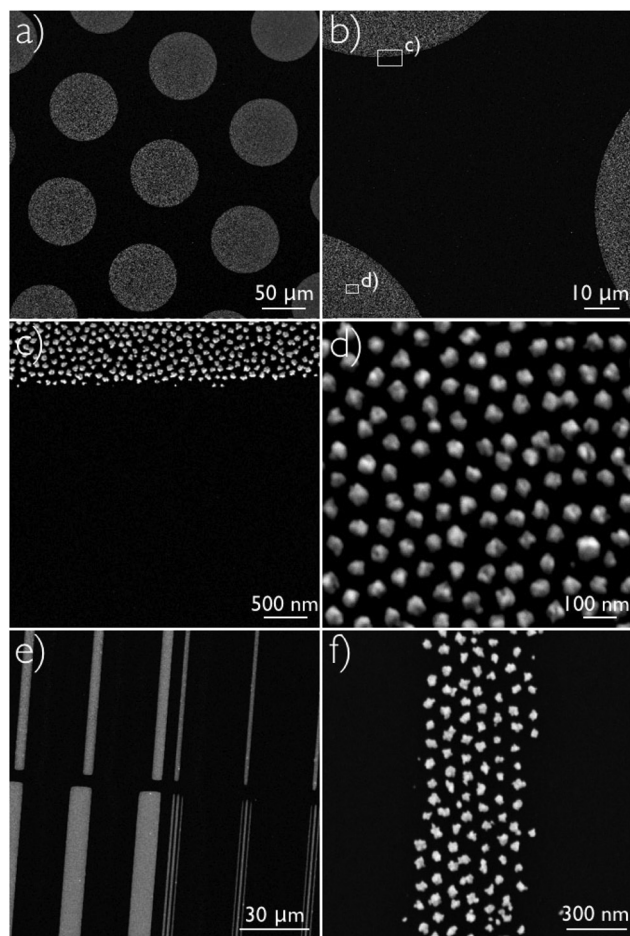


Fig. 3 Micelle templated photochemistry enables the micropatterning of gold potatoids. SEM images display various circular and linear micropatterns of gold potatoids at different magnifications. (c) and (d) Correspond to areas indicated in (b) and imaged at higher magnifications.

By increasing ED time, the absorbance of nanoring arrays becomes more intense but undergoes after 90 min a blue shift to 640 nm. This is due to the increase of the ring thickness ranging from 18 to 35 nm, which turns nanorings into structures with optical properties similar to the ones of randomly shaped nanoparticles (Fig. 5). The order of the two last proces-

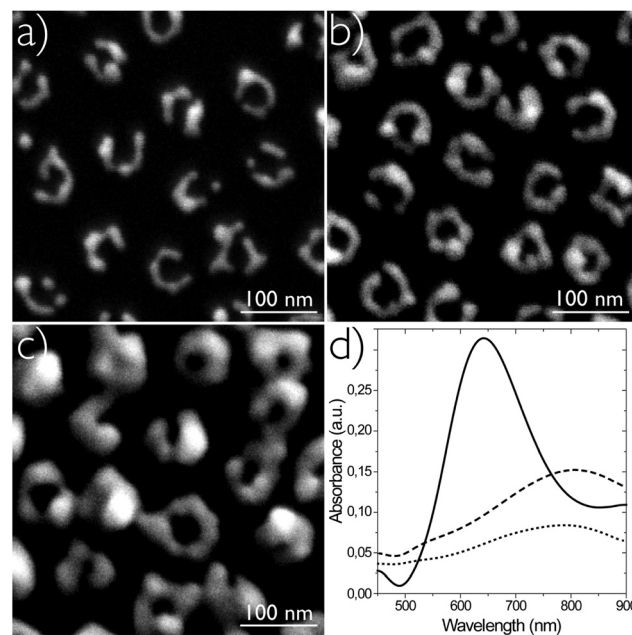


Fig. 5 Tuning the surface plasmon resonance of nanoring arrays with ED time. SEM images of nanorings grown for (a) 10, (b) 30 and (c) 90 min in a mixture of gold aqueous solution and ethanalamine. (d) Extinction spectra measured in air of gold nanorings grown for 10 (dots), 30 (dashes) and 90 min (line).

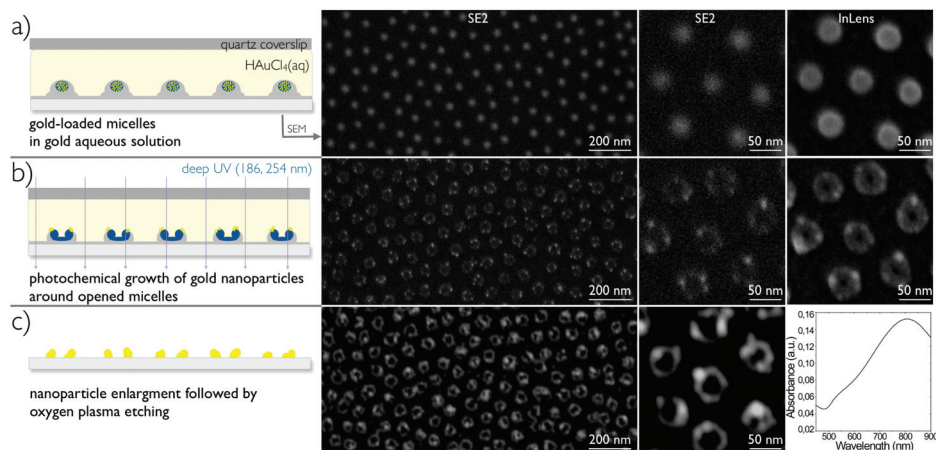


Fig. 4 Micellar photochemical lithography to fabricate gold nanoring arrays. Schematics and SEM images illustrating the evolution of the nanostructured substrate after each processing step: upon (a) flattening a drop of gold aqueous solution, (b) deep UV illumination and (c) electroless deposition followed by O_2 plasma etching. The extinction spectrum measured in air of the gold nanoring array is displayed in the lower right corner.

sing steps proved again to be critical for shaping gold nanoparticles as the inverted order leads to the circular assembly of individual dots and small aggregates mainly absorbing at 530 and 640 nm, respectively (Fig. S5a and b†).

To identify which experimental parameters mediate the structure reconstruction from spherical to pitted micelles, we tested our procedure while using monochromatic illumination ($\lambda = 254$ nm, 20 W). During the irradiation step, no morphological change was observed and gold growth occurred in 75% of micelles decorated with only one or two nanoparticles (Fig. S7†). Upon ED and plasma etching, arrays of spherical particles with a diameter of about 10 and 35 nm were obtained (Fig. S7b†). This observation indicates that 185 nm light efficiently mediates gold growth while partially oxidizing or etching the thin PS micellar shell,³⁸ so that P2VP chains are exposed to the liquid interface and partly shield PS to finally form pores.⁵⁴ Solubilized gold anions also play an active role in this process, as micelle opening did not take place upon irradiating micelles in water (Fig. 1). Unfortunately, we did not observe micelle opening upon micropatterning the substrate. By using a photomask, a sufficient UV dose may not be reached for triggering this process, thereby leading to the formation of potatooids (data not shown).

In comparison to other pore-making strategies for which one of the two polymer blocks is either etched away by physical means or reconstructed in presence of selective solvents,⁵⁷ our approach requires both mechanisms since the morphology of gold-loaded micelles is more difficult to manipulate than unloaded ones. Nevertheless, our strategy enables the fabrication of uniform nanoring arrays that feature a localized plasmon resonance in the near-infrared, whereas other BCML-based methods report the preparation of ring-like structures made of assembled nanoparticles, which were not optically characterized.^{58–61}

Optical and photothermal properties of nanostructured gold rings and potatooids

Let us finally focus on the particular optical properties of the reported gold nanostructures and their relative benefits in comparison to plasmonic structures fabricated with physical methods. The main benefit we envision concerns their photothermal properties. We have already shown that arrays of spherical nanoparticles generated by BCML have proven to be valuable substrates in thermoplasmonics,^{38,62–64} and assemblies of nanorings and potatooids make no exception. In nanoplasmonics, the incident light interacting with nanoparticles is scattered and/or absorbed, and the sum of these two processes is referred to as extinction. Among these three processes, absorption is the process of interest for applications in thermoplasmonics as it is the origin of the desired local temperature increase during illumination. To quantify the photothermal properties of the BCML substrates, we used the thermal microscopy imaging technique that we recently developed and named TIQSI (thermal imaging using quadriwave lateral shearing interferometry).⁶⁴ This technique enables the mapping of temperature and heat source density around gold

nanoparticles lying upon a planar substrate (Fig. S8†). TIQSI also allows retrieving the absorption of the sample by integrating the heat source map and dividing the result by the incident laser power.⁶⁴ We performed such measurements for a set of wavelengths ranging from 711 nm to 864 nm (as permitted by our Ti-Sapphire laser) in order to reconstruct a quantitative absorption spectrum of the samples. In parallel, we performed quantitative extinction measurement in water by measuring the light intensity (I) crossing the substrate in two conditions: (I_1) with and (I_2) without gold nanoparticles. Extinction is then simply obtained using $\text{ext} = (I_2 - I_1)/I_2$. Finally, scattering can be quantified by subtracting extinction and absorption measurements.

As revealed by the measurements made in water, rings and potatooids feature a red-shifted surface plasmon resonance in comparison to the ones measured in air (Fig. 1d and 4c) and a great absorption-scattering ratio (Fig. 6a and d). Ring-like structures are even purely absorbing (Fig. 6a), *i.e.* negligible scattering occurs, and potatooids feature an absorption-scatter-

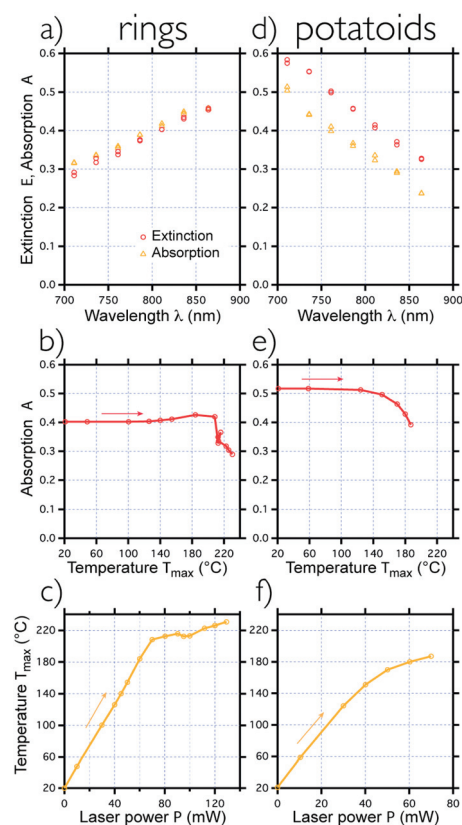


Fig. 6 Optical and photothermal properties of gold nanorings and potatooids in water. (a) Extinction and absorption of an array of nanorings (ED 30 min) as a function of the wavelength. (b) Absorption of an area of the nanorings measured after a 5-second laser exposure ($\lambda = 786$ nm), plotted as a function of the maximum temperature achieved during illumination. The arrow indicates the direction of the successive measurements. (c) Maximum temperature achieved as a function of the laser power. (d), (e) and (f) Correspond to the same series of measurements as (a), (b), and (c) for a potatooid nanoarray (ED 40 min, $\lambda = 736$ nm).

ing ratio of around 5 (Fig. 6d). This feature is rare in plasmonics in the near infrared, albeit beneficial for photothermal applications. For instance, plasmonic structures made by electron beam and colloidal lithography scatter a large fraction of the incident light due to their larger size, making them poor absorbers.⁶⁵

We have recently shown that very high temperature increases can be achieved in aqueous solution far above the boiling point of the surrounding fluid at the vicinity of spherical gold nanoparticles synthesized by BCML (220 °C in water).⁶³ This phenomenon is termed superheating and occurs when no nucleation point for vapour bubble formation is present in the heated region. In this context, we have investigated the temperature sustainability of such substrates up to the temperature threshold for bubble formation (around 200 °C). In order to evidence any temperature-induced damage of the specimens, we measured the absorption of the samples subsequent to a 5-second illumination as a function of the temperature generated by the nanoparticle arrays. For these measurements, we considered the temperature at the centre of the illuminated area, *i.e.* the maximum temperature observed in the temperature maps (Fig. S8c†). Nanorings were stable up to around 200 °C (Fig. 6b and c), although a slight increase of the absorbance was observed from 130 °C, probably due a small change of the nanoparticle morphology. Potatoids were less stable as the absorbance tends to drop from 120 °C and the nanoparticles may detach from the substrate at around 190 °C as the absorbance decreases (Fig. 6e and f). In both cases, the reported gold structures are stable above the water boiling point and enable superheating. This observation means that nanorings and potatoids do not act as nucleation points. This conclusion opens the path for future applications involving near-infrared-induced thermal processes using potatoids and nanorings made by BCML.

Conclusions

We described a straightforward and cost-effective photochemical method to fabricate uniform arrays of gold nanoparticles on glass with micro/nanometric spatial resolution without requiring any additional photosensitizers or photoresists. By using block copolymer micellar monolayers as reactive templates, we fabricated plasmonic substrates with tuneable surface plasmon resonances. Depending on the extra-micellar chemical environment and the illumination wavelength, we succeeded in patterning and shaping optically active nanostructures such as gold potatoids and rings of about 50 nm in diameter that feature localized plasmon resonances above 600 and 800 nm, respectively. Quantification of their photothermal properties showed that nanoring-based substrates are temperature-resistant and features ideal photothermal properties, opening the path for future applications controlled by near-infrared light, including nanoscale solvothermal synthesis and spatiotemporal manipulation of biological systems within the tissue transparency window.

Acknowledgements

We thank R. Fässler for support. The Max Planck Society financially supported this work.

References

- 1 M. Daniel and D. Astruc, *Chem. Rev.*, 2004, **104**, 293–346.
- 2 P. K. Jain, K. S. Lee, I. H. El-Sayed and M. A. El-Sayed, *J. Phys. Chem. B*, 2006, **110**, 7238–7248.
- 3 S. E. Lohse and C. J. Murphy, *Chem. Mater.*, 2013, **25**, 1250–1261.
- 4 N. J. Halas, S. Lal, W.-S. Chang, S. Link and P. Nordlander, *Chem. Rev.*, 2011, **111**, 3913–3961.
- 5 M. A. Mahmoud, D. O'Neil and M. A. El-Sayed, *Chem. Mater.*, 2014, **26**, 44–58.
- 6 Y. Jin, *Adv. Mater.*, 2012, **24**, 5153–5165.
- 7 B. Yan, S. V. Boriskina and B. M. Reinhard, *J. Phys. Chem. C*, 2011, **115**, 24437–24453.
- 8 G. Baffou and R. Quidant, *Laser Photon. Rev.*, 2013, **7**, 171–187.
- 9 E. Boulais, R. Lachaine, A. Hatf and M. Meunier, *J. Photochem. Photobiol., C*, 2013, **17**, 26–49.
- 10 R. Near, C. Tabor, J. Duan, R. Pachter and M. El-Sayed, *Nano Lett.*, 2012, **12**, 2158–2164.
- 11 G. Zhang and D. Wang, *Chem. – Asian J.*, 2009, **4**, 236–245.
- 12 Y. Li, W. Cai and G. Duan, *Chem. Mater.*, 2008, **20**, 615–624.
- 13 S. Ullrich, S. P. Scheeler, C. Pacholski, J. P. Spatz and S. Kuder, *Part Part. Syst. Charact.*, 2012, **30**, 102–108.
- 14 M. B. Müller, C. Kuttner, T. A. F. König, V. V. Tsukruk, S. Förster, M. Karg and A. Fery, *ACS Nano*, 2014, **8**, 9410–9421.
- 15 L. Wang, F. Montagne, P. Hoffmann, H. Heinzelmann and R. Pugin, *J. Colloid Interface Sci.*, 2011, **356**, 496–504.
- 16 C. Farcau, N. M. Sangeetha, N. Decorde, S. Astilean and L. Ressler, *Nanoscale*, 2012, **4**, 7870.
- 17 J. Fontana, J. Livenere, F. J. Bezares, J. D. Caldwell, R. Rendell and B. R. Ratna, *Appl. Phys. Lett.*, 2013, **102**, 201606.
- 18 W. Lee, S. Y. Lee, R. M. Briber and O. Rabin, *Adv. Funct. Mater.*, 2011, **21**, 3424–3429.
- 19 L. Vigderman, B. P. Khanal and E. R. Zubarev, *Adv. Mater.*, 2012, **24**, 4811–4841.
- 20 M. Mueller, M. Tebbe, D. V. Andreeva, M. Karg, R. A. Alvarez-Puebla, N. Pazos Perez and A. Fery, *Langmuir*, 2012, **28**, 9168–9173.
- 21 M. Park, C. Harrison, P. Chaikin, R. Register and D. Adamson, *Science*, 1997, **276**, 1401–1404.
- 22 S. B. Darling, *Prog. Polym. Sci.*, 2007, **32**, 1152–1204.
- 23 S. Forster, *Top. Curr. Chem.*, 2003, **226**, 1–28.
- 24 C. Brinker, Y. Lu, A. Sellinger and H. Fan, *Adv. Mater.*, 1999, **11**, 579.
- 25 F. L. Yap, P. Thoniyot, S. Krishnan and S. Krishnamoorthy, *ACS Nano*, 2012, **6**, 2056–2070.

- 26 W. J. Cho, Y. Kim and J. K. Kim, *ACS Nano*, 2012, **6**, 249–255.
- 27 W. Lopes and H. Jaeger, *Nature*, 2001, **414**, 735–738.
- 28 J. Y. Cheng, C. A. Ross, V. Chan, E. L. Thomas, R. Lammertink and G. J. Vancso, *Adv. Mater.*, 2001, **13**, 1174.
- 29 I. Vukovic, G. ten Brinke and K. Loos, *Polymer*, 2013, **54**, 2591–2605.
- 30 T. Thurn-Albrecht, J. Schotter, C. A. Kastle, N. Emley, T. Shibauchi, L. Krusin-Elbaum, K. Guarini, C. T. Black, M. T. Tuominen and T. P. Russell, *Science*, 2000, **290**, 2126–2129.
- 31 H.-S. Moon, J. Y. Kim, H. M. Jin, W. J. Lee, H. J. Choi, J. H. Mun, Y. J. Choi, S. K. Cha, S. H. Kwon and S. O. Kim, *Adv. Funct. Mater.*, 2014, **24**, 4343–4348.
- 32 Y. Wang, M. Becker, L. Wang, J. Liu, R. Scholz, J. Peng, U. Gösele, S. Christiansen, D. H. Kim and M. Steinhart, *Nano Lett.*, 2009, **9**, 2384–2389.
- 33 M. Aizawa and J. M. Buriak, *Chem. Mater.*, 2007, **19**, 5090–5101.
- 34 L. A. Porter, H. C. Choi, J. M. Schmeltzer, A. E. Ribbe, L. C. C. Elliott and J. M. Buriak, *Nano Lett.*, 2002, **2**, 1369–1372.
- 35 T. Brezesinski, M. Groenewolt, A. Gibaud, N. Pinna, M. Antonietti and B. M. Smarsly, *Adv. Mater.*, 2006, **18**, 2260.
- 36 J. Polleux, M. Rasp, I. Louban, N. Plath, A. Feldhoff and J. P. Spatz, *ACS Nano*, 2011, **5**, 6355–6364.
- 37 G. Kastle, H. Boyen, F. Weigl, G. Lengl, T. Herzog, P. Ziemann, S. Riethmuller, O. Mayer, C. Hartmann, J. Spatz, M. Moller, M. Ozawa, F. Banhart, M. Garnier and P. Oelhafen, *Adv. Funct. Mater.*, 2003, **13**, 853–861.
- 38 M. Zhu, G. Baffou, N. Meyerbröcker and J. Polleux, *ACS Nano*, 2012, **6**(8), 7227–7233.
- 39 J. Chai, D. Wang, X. Fan and J. M. Buriak, *Nat. Nanotechnol.*, 2007, **2**, 500–506.
- 40 J. Chai and J. M. Buriak, *ACS Nano*, 2008, **2**, 489–501.
- 41 Y. Liu, K. Yehl, Y. Narui and K. Salaita, *J. Am. Chem. Soc.*, 2013, **135**, 5320–5323.
- 42 T. Lohmueller, D. Aydin, M. Schwieder, C. Morhard, I. Louban, C. Pacholski and J. P. Spatz, *Biointerphases*, 2011, **6**, MR1–MR12.
- 43 N. G. Caculitan, H. Kai, E. Y. Liu, N. Fay, Y. Yu, T. Lohmüller, G. P. O'Donoghue and J. T. Groves, *Nano Lett.*, 2014, **14**, 2293–2298.
- 44 A. J. Mieszawska, G. W. Slawinski and F. P. Zamborini, *J. Am. Chem. Soc.*, 2006, **128**, 5622–5623.
- 45 A. J. Mieszawska and F. P. Zamborini, *Chem. Mater.*, 2005, **17**, 3415–3420.
- 46 S. Kumar, H. Yang and S. Zou, *J. Phys. Chem. C*, 2007, **111**, 12933–12938.
- 47 N. Taub, O. Krichevski and G. Markovich, *J. Phys. Chem. B*, 2003, **107**, 11579–11582.
- 48 L. Osinkina, T. Lohmüller, F. Jäckel and J. Feldmann, *J. Phys. Chem. C*, 2013, **117**, 22198–22202.
- 49 M. Sakamoto, M. Fujistuka and T. Majima, *J. Photochem. Photobiol., C*, 2009, **10**, 33–56.
- 50 J. C. Scaiano, K. G. Stamplecoskie and G. L. Hallett-Tapley, *Chem. Commun.*, 2012, **48**, 4798.
- 51 S. Eustis and M. A. El-Sayed, *J. Phys. Chem. B*, 2006, **110**, 14014–14019.
- 52 K. L. McGilvray, J. Granger, M. Correia, J. T. Banks and J. C. Scaiano, *Phys. Chem. Chem. Phys.*, 2011, **13**, 11914.
- 53 V. Kochat, A. N. Pal, E. S. Sneha, A. Sampathkumar, A. Gairola, S. A. Shivashankar, S. Raghavan and A. Ghosh, *J. Appl. Phys.*, 2011, 110.
- 54 Z. Chen, C. He, F. Li, L. Tong, X. Liao and Y. Wang, *Langmuir*, 2010, **26**, 8869–8874.
- 55 K. Koga, T. Ikeshoji and K.-I. Sugawara, *Phys. Rev. Lett.*, 2004, **92**, 115507.
- 56 J. Chen, P. Mela, M. Moeller and M. C. Lensen, *ACS Nano*, 2009, **3**, 1451–1456.
- 57 Y. Wang and F. Li, *Adv. Mater.*, 2011, **23**, 2134–2148.
- 58 L. Wang, F. Montagne, P. Hoffmann and R. Pugin, *Chem. Commun.*, 2009, 3798.
- 59 X. Zu, X. Hu, L. A. Lyon and Y. Deng, *Chem. Commun.*, 2010, **46**, 7927.
- 60 J.-H. Ryu, S. Park, B. Kim, A. Klaiherd, T. P. Russell and S. Thayumanavan, *J. Am. Chem. Soc.*, 2009, **131**, 9870–9871.
- 61 H. Cho, S. Choi, J. Y. Kim and S. Park, *Nanoscale*, 2011, **3**, 5007.
- 62 G. Baffou, P. Berto, E. Bermúdez Ureña, R. Quidant, S. Monneret, J. Polleux and H. Rigneault, *ACS Nano*, 2013, **7**, 6478–6488.
- 63 G. Baffou, J. Polleux, H. Rigneault and S. Monneret, *J. Phys. Chem. C*, 2014, **118**, 4890–4898.
- 64 G. Baffou, P. Bon, J. Savatier, J. Polleux, M. Zhu, M. Merlin, H. Rigneault and S. Monneret, *ACS Nano*, 2012, **6**, 2452–2458.
- 65 H.-Y. Tseng, W.-F. Chen, C.-K. Chu, W.-Y. Chang, Y. Kuo, Y.-W. Kiang and C. C. Yang, *Nanotechnology*, 2013, **24**, 065102.